Trimming of silicon ring resonator by electron beam induced compaction and strain

J. Schrauwen, D. Van Thourhout, and R. Baets

Photonics Research Group, Department of Information Technology, Ghent University - IMEC, B-9000 Gent, Belgium
jonathan.schrauwen@intec.ugent.be

Abstract: Silicon is becoming the preferable platform for future integrated components, mostly due to the mature and reliable fabrication capabilities of electronics industry. Nevertheless, even the most advanced fabrication technologies suffer from non-uniformity on wafer scale and on chip scale, causing variations in the critical dimensions of fabricated components. This is an important issue since photonic circuits, and especially cavities such as ring resonators, are extremely sensitive to these variations. In this paper we present a way to circumvent these problems by trimming using electron beam induced compaction of oxide in silicon on insulator. Volume compaction of the oxide cladding causes both changes in the refractive index and creates strain in the silicon lattice. We demonstrate a resonance wavelength red shift 4.91 nm in a silicon ring resonator.

OCIS codes: (230.3120) Integrated optics Devices; (130.7408) Wavelength filtering devices

References and links

1. T. Tsuchizawa, K. Yamada, H. Fukuda, T. Watanabe, J. Takahashi, M. Takahashi, T. Shoji, E. Tamechika, S. Itabashi, and H. Morita, "Microphotonics devices based on silicon microfabrication technology," IEEE J. Sel. Top. Quantum Electron. **11**, 232-240 (2005).
2. Q. F. Xu, B. Schmidt, S. Pradhan, and M. Lipson, "Micrometre-scale silicon electro-optic modulator," Nature **435**, 325-327 (2005).
3. P. Dumon, W. Bogaerts, D. Van Thourhout, D. Taillaert, R. Baets, J. Wouters, S. Beckx, and P. Jaenen, "Compact wavelength router based on a Silicon-on-insulator arrayed waveguide grating pigtailed to a fiber array," Opt. Express **14**, 664-669 (2006).
4. H. S. Rong, R. Jones, A. S. Liu, O. Cohen, D. Hak, A. Fang, and M. Paniccia, "A continuous-wave Raman silicon laser," Nature **433**, 725-728 (2005).
5. G. Roelkens, D. Van Thourhout, R. Baets, R. Notzel, and M. Smit, "Laser emission and photodetection in an InP/InGaAsP layer integrated on and coupled to a Silicon-on-Insulator waveguide circuit," Opt. Express **14**, 8154-8159 (2006).
6. A. W. Fang, R. Jones, H. Park, O. Cohen, O. Raday, M. J. Paniccia, and J. E. Bowers, "Integrated AlGaInAs-silicon evanescent racetrack laser and photodetector," Opt. Express **15**, 2315-2322 (2007).
7. J. Van Campenhout, P. Rojo Romeo, P. Regreny, C. Saessal, D. Van Thourhout, S. Verstuyft, L. Di Cioccio, J.-M. Fedeli, C. Lagahe, and R. Baets, "Electrically pumped InP-based microdisk lasers integrated with a nanophotonic silicon-on-insulator waveguide circuit," Opt. Express **15**, 6744-6749 (2007).
8. P. Dumon, W. Bogaerts, V. Wiaux, J. Wouters, S. Beckx, J. Van Campenhout, D. Taillaert, B. Luyssaert, P. Bienstman, D. Van Thourhout, and R. Baets, "Low-loss SOI photonic wires and ring resonators fabricated with deep UV lithography," IEEE Photon. Technol. Lett. **16**, 1328-1330 (2004).
9. Y. Akahane, T. Asano, B. S. Song, and S. Noda, "High-Q photonic nanocavity in a two-dimensional photonic crystal," Nature **425**, 944-947 (2003).
10. W. Bogaerts, D. Taillaert, B. Luyssaert, P. Dumon, J. Van Campenhout, P. Bienstman, D. Van Thourhout, R. Baets, V. Wiaux, and S. Beckx, "Basic structures for photonic integrated circuits in silicon-on-insulator," Opt. Express **12**, 1583-1591 (2004).
11. I. Kiyat, A. Aydinli, and N. Dagli, "Low-power thermooptical tuning of SOI resonator switch," IEEE Photon. Technol. Lett. **18**, 364-366 (2006).
12. E. J. Klein, D. H. Geuzebroek, H. Kelderman, G. Sengo, N. Baker, and A. Driessen, "Reconfigurable optical add-drop multiplexer using microring resonators," IEEE Photon. Technol. Lett. **17**, 2358-2360 (2005).
13. Y. Nasu, M. Kohtoku, M. Abe, and Y. Hibino, "Birefringence suppression of UV-induced refractive index with grooves in silica-based planar lightwave circuits," Electron. Lett. **41**, 1118-1119 (2005).
14. H. Haeiwa, T. Naganawa, and Y. Kokubun, "Wide range center wavelength trimming of vertically coupled microring resonator filter by direct UV irradiation to SiN ring core," IEEE Photon. Technol. Lett. **16**, 135-137 (2004).

15. S. Ueno, T. Naganawa, and Y. Kokubun, "High UV sensitivity of SiON film and its application to center wavelength trimming of microring resonator filter," IEICE Trans. Electron. **E88c**, 998-1004 (2005).
16. A. J. Houghton, and P. D. Townsend, "Optical-waveguides formed by low-energy electron-irradiation of silica," Appl. Phys. Lett. **29**, 565-566 (1976).
17. D. Barbier, M. Green, and S. J. Madden, "Wave-guide fabrication for integrated-optics by electron-beam irradiation of silica," J. Lightwave Technol. **9**, 715-720 (1991).
18. S. Garcia-Blanco, and J. S. Aitchison, "Direct electron beam writing of optical devices on Ge-doped flame hydrolysis deposited silica," IEEE J. Sel. Top. Quantum Electron. **11**, 528-538 (2005).
19. M. Svalgaard, C. V. Poulsen, A. Bjarklev, and O. Poulsen, "Direct Uv writing of buried singlemode channel wave-guides in Ge-doped silica films," Electron. Lett. **30**, 1401-1403 (1994).
20. D. A. Zauner, J. Hubner, K. J. Malone, and M. Kristensen, "UV trimming of arrayed-waveguide grating wavelength division demultiplexers," Electron. Lett. **34**, 780-781 (1998).
21. H. N. J. Fernando, J. Canning, L. Wosinski, B. Jaskorzynska, and M. Dainese, "Characterization of ultra-violet-induced changes in planar waveguides," J. Opt. A Pure Appl. Opt. **5**, 335-340 (2003).
22. W. Primak, and R. Kampwirth, "The radiation compaction of vitreous silica," J. Appl. Phys. **39**, 5651-5658 (1968).
23. W. Primak, "Mechanism for radiation compaction of vitreous silica," J. Appl. Phys. **43**, 2745 (1972).
24. C. B. Norris and E. P. Eernisse, "Ionization dilatation effects in fused silica from 2 to 18-Kev electron-irradiation," J. Appl. Phys. **45**, 3876-3882 (1974).
25. F. Piao, W. G. Oldham, and E. E. Haller, "The mechanism of radiation-induced compaction in vitreous silica," J. Non-Cryst. Solids **276**, 61-71 (2000).
26. K. De Vos, I. Bartolozzi, E. Schacht, P. Bienstman, and R. Baets, "Silicon-on-insulator microring resonator for sensitive and label-free biosensing," Opt. Express **15**, 7610-7615 (2007).
27. D. Taillaert, W. Van Paepegem, J. Vlekken, and R. Baets, "A thin foil optical strain gage based on silicon-on-insulator microresonators," Third European Workshop on Optical Fibre Sensors (EWOFS 2007) **6619**, 661914 (2007).
28. T. A. Dellin, D. A. Tichenor, and E. H. Barsis, "Surface Compaction in Irradiated Vitreous Silica," Bulletin of the American Physical Society **21**, 296-296 (1976).

1. Introduction

Silicon-on-insulator (SOI) is gaining interest as preferable material system for future ultra-compact integrated photonic components. The main advantages of this material system are firstly the high refractive index contrast between silicon (core) and oxide or air (cladding) enabling small bend radii and dense integration, and secondly mature fabrication facilities thanks to the electronics industry. In spite of the indirect band gap of silicon, both passive [1-3] and active [4-7] devices have been demonstrated thanks to heterogeneous integration of III-V semiconductors. One of the applications aimed for by the telecom industry is optical filters for wavelength (de)multiplexing. SOI is the ideal platform to make these filters compact and low-cost. Several geometries, such as ring resonators [8] and photonic band gap materials [9] have good filtering characteristics. However, most of the demonstrated filters were fabricated with electron beam lithography, which is a serial fabrication technique and therefore unattractive for mass fabrication. In previous work we have demonstrated that these filters can also be fabricated in a parallel way, with 248 nm Deep-UV lithography (DUV) in a standard Complementary Metal Oxide Semiconductor (CMOS) facility [10]. However, variations of the critical dimensions of devices fabricated by optical lithography are inevitable. These variations can be caused by wafer non-uniformity, by e.g. varying layer thicknesses on wafer edges, or by non-uniformity within one chip, mainly caused by lithography imperfections near mask edges. A way to assess critical dimension variations in a photonic circuit is to evaluate the resonance wavelength shift of identically designed ring resonators, dispersed over a wafer. These resonators can be fabricated with Q-factors of about 10^4 [8], or a 3 dB bandwidth of 0.15 nm. In practice the resonance wavelength shifts exceed 1 nm, which is unacceptable for many applications. The most common solution for this is active thermal tuning [11, 12], however, when many resonators have to be integrated on a single chip, this would lead to high power consumption and important device complexity. Another approach to circumvent these process variations is trimming of the devices after fabrication. In this paper we present a technique to locally and independently trim the resonances of ring resonators on a silicon chip. This allows for complete compensation of resonance wavelength variations on silicon photonic integrated components.

2. Electron beam induced compaction of the SiO_2 cladding

The resonance wavelength of a ring resonator is trimmed by changing the optical path length of the resonator, in our case by varying the effective index of the guided mode and not the length of the ring. An increase in effective index causes a red shift of the resonance wavelength. This was demonstrated in several (low to medium index contrast) material systems such as silica glass [13] and SiN/SiON [14, 15]. These core materials are sensitive to either UV or electron beam compaction (also other higher energy particles tend to compact these materials, but these are less commercially practicable). This means that the compacted material contains most of the optical mode and thus relatively large shifts in effective indices can be obtained. In SiN more than 10 nm of resonance wavelength shift was obtained for ring resonators operating at 1550 nm [14]. Electron beam [16-18] as well as UV [19-21] irradiation have been used to fabricate or alter waveguides in silica glass. In SOI, the preferable material system for future industrial deployment, the core material is silicon, which can not be compacted by either UV or electrons. Only the SiO_2 cladding is susceptible to compaction. Literature reports on SiO_2 volume compaction and refractive index changes upon irradiation with highly energetic particles. The particles include ions and gamma photons, by which the oxide compacts due to knock-on atom displacements, or electrons and UV photons, where the compaction is caused by ionization-induced relaxation of inherently strained Si-O bonds in the glass network [22-25]. Due to the imaging capabilities and the ease to precisely control the irradiation dose and energy we have used an electron beam (from an FEI Nova 600 scanning ion/electron microscope) to compact the SiO_2 cladding layer. The experiments presented here differ from previous reports in the fact that the optical core material – silicon – can not be compacted, thus strain induced by cladding compaction is used as trimming mechanism.

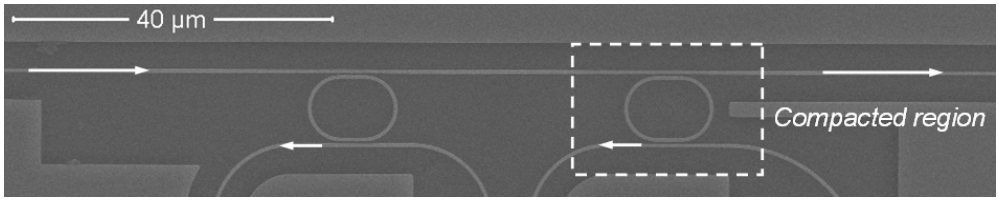

Fig. 1. Overview of the experiment: the right ring is trimmed by electron beam compaction; the left one is kept original as a reference to exclude temperature or ambient variations.

3. Experiment: 4.91 nm red shift of a silicon ring resonator

The resonance frequency of silicon ring resonators is extremely sensitive to changes of temperature and of the surrounding medium; rings are therefore attractive as sensors [26, 27]. However, in this experiment we want to exclude all external factors and investigate the resonance shifts caused only by electron beam irradiation. Therefore we have fabricated a sample with two rings, with different resonance wavelengths, serially connected to the same waveguide, as depicted in Fig. 1. Only one of these rings is irradiated by imaging it with a scanning electron beam. The transmission spectrum features two superimposed ring spectra. By evaluating only relative peak shifts between the two ring spectra the external influences are excluded. The experiment was performed in situ, inside the vacuum chamber of a scanning electron microscope, by providing it with vacuum fiber feedthroughs. The optical input and output signals are transported by single mode fibers, glued (with UV-curable glue) in a near-vertical position above grating couplers. The optical circuit, with grating couplers, waveguides, tapering sections, and ring resonators, was fabricated by DUV lithography in a standard CMOS foundry [10]. Light was generated by a super luminescent LED with center wavelength at 1530 nm and detected by a spectrum analyzer with a resolution of 60 pm.

The right ring resonator was trimmed in three subsequent steps, as depicted in Fig. 2. In a first step we have scanned a 0.21 nA beam across a 25.6 µm x 22.1 µm area for 360 s, and

measured a resonance wavelength shift of 1.24 nm. In the next step the same beam was scanned over the same area for 300 s to reach an extra shift of 0.82 nm. In a final step a 0.84 nA beam was scanned over a 17.1 µm x 14.8 µm area for 400 s, leading to a subsequent shift of 2.77 nm. In total this leads to a 4.91 nm red shift of the resonance wavelength of the silicon ring. Figure 2 shows the evolution of the resonance peaks, extracted from the measured spectra (one spectrum was measured every 10 s). In the final step the resonance wavelength of the right ring was equated with that of the left ring. To evaluate the propagation losses we have extracted the Q-factors from the measured spectra, as depicted in Fig. 2. It is clear that the Q-factor slightly decreases in the third step of the experiment, which is also visible in the right part of Fig. 2. We argue that the increase during the second step is caused by a varying coupling constant, whereas the decrease in the third step is caused by increasing propagation losses.

It is clear from the graph that in the beginning of the electron beam exposure there is a small blue shift of the resonance (between 100 pm and 200 pm blue shift in our experiments), and after the exposure there is settling of the peak towards longer wavelengths (we have measured 153 pm red shift, 45 minutes after the second step). We argue that this is partly caused by charging of the oxide and subsequent generation of carriers in the silicon, and partly by temperature variations due to electron bombardment. It was reported [24] that compacted silica tends to relax over a period of tens of hours after irradiation. However, we have measured a subsequent red shift of 0.15 nm, 5 days after the actual irradiation. This effect needs further investigation.

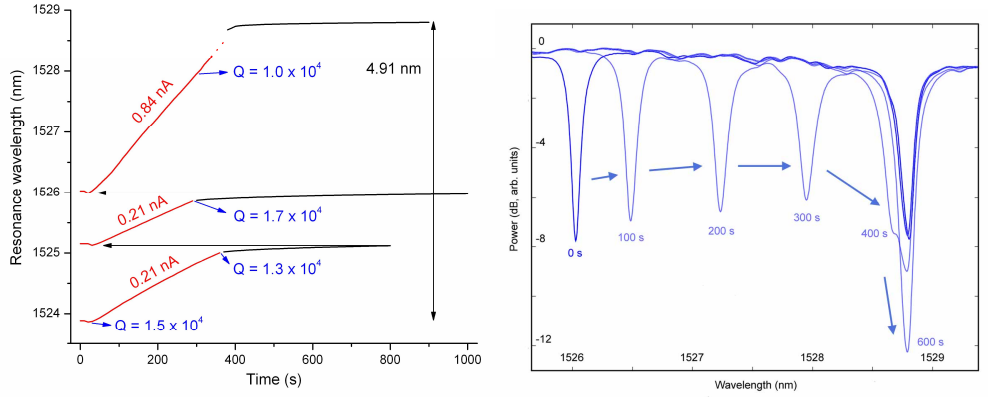

Fig. 2 Left: Three subsequent steps were used to equate the resonance wavelength of the right ring resonator with that of the left ring resonator. The curves represent the position of the fitted peak maxima. The grey lines (color online: red) indicate the actual electron beam irradiation; the black lines show the settling after irradiation. The dotted red line is the region where both resonance peaks merge and our single peak fitting algorithm yields inconclusive results. The Q-factors of the trimmed ring during the three steps of the experiment were extracted from the measured spectra. Right: Evolution of the resonance during the third stage of the experiment. The Q-factor of the trimmed ring decreases from 1.7 x 10^4 at 1526 nm to 1.0 x 10^4 at 1528 nm.

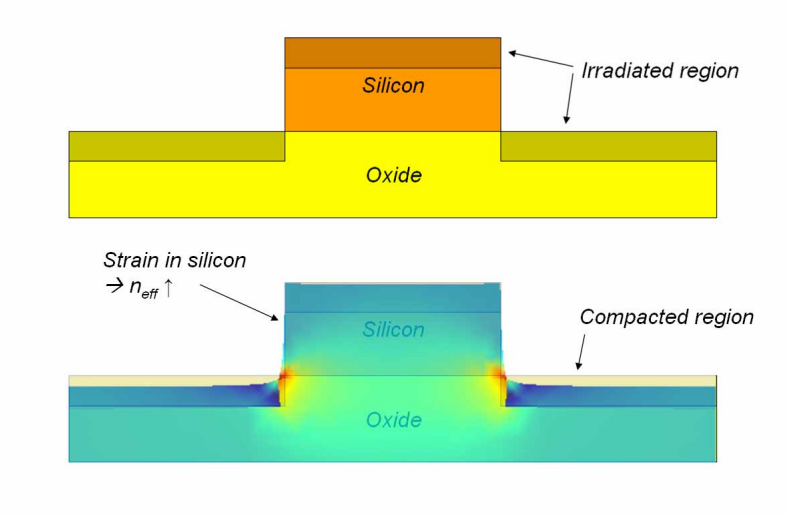

Fig. 3. Cross-section of the 220 nm thick silicon ring resonator. The 2 keV electrons penetrate 70 nm into silicon and oxide, and lead to volume compaction only in the oxide. This effect generates a tensile strain in the silicon, parallel to the substrate. The effect of silicon strain dominates the refractive index change. In the bottom drawing the first principal strain obtained from a finite element simulation was overlaid. (Color online: dark blue = compressive strain 0.05; red = tensile strain 0.17)

4. Discussion: cladding refractive index change versus core compaction-induced stress

Two distinct physical processes cause the effective index change of the mode in the silicon ring resonator, as depicted in Fig. 3. The first is a larger refractive index of the oxide cladding due to volume compaction; the second is the stress this oxide compaction induces in the silicon lattice. In our experiment we have worked with 2 keV electrons, which have a penetration depth of about 70 nm in Si and SiO_2 (this was calculated with Monte Carlo simulations, and confirmed by [24]). The silicon ring is 220 nm thick, on top of a 2 μm oxide layer; therefore the electrons can not penetrate the silicon. The mode overlap with the compacted oxide is lower than 1.5%, as was calculated with a mode expansion tool. From [24, 28] we have estimated the maximum amount of refractive index change to be below 3% (i.e. for a compaction of about 10%), with a total irradiation dose of 2.8 x 10^{23} keV/cm^3 (the total dose in our experiment). This can not lead to more than 0.5 nm shift in resonance wavelength. We can thus conclude that the largest fraction of the observed resonance wavelength shift is caused by strain in the silicon lattice. Finite elements simulations were used to evaluate this effect (with a variable mesh size, down to 10 nm where a large stress gradient is reached), as shown in Fig. 3. The overlay picture illustrates the deformed mesh (with a scale factor of 2) and the first principal strain in the case of a 10% compacted oxide layer with a thickness of 70 nm.

It was reported [28] that the induced stress in the compacted oxide layer saturates upon high dose electron beam irradiation. However, we have not found reports of this effect for the energy and dose range considered in our experiments. Since a complete study was beyond the scope of this work, we have chosen to estimate the influence of compaction induced stress on the effective index of the supported modes without detailed simulations of the optical mode profile in the strained lattice. We have therefore calculated the average silicon strain in the dominant direction: perpendicular to the waveguide propagation direction and in the plane of the substrate surface. The resonance wavelength shift was calculated by using only the p_{11} component of the silicon elasto-optical tensor. This shift is calculated for varying oxide compaction rates and for different compacted layer thicknesses. The results, displayed in Fig. 4, support the fact that tensile strain in the silicon waveguide can account for the observed resonance wavelength shift.

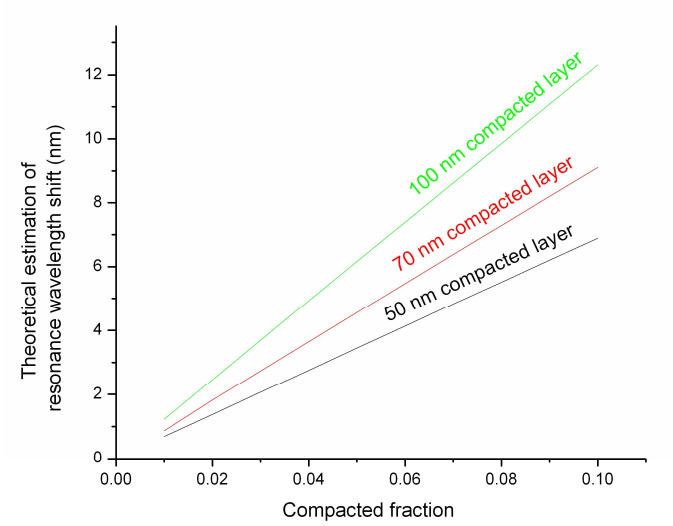

Fig. 4. Calculated resonance wavelength shift due to strain in the silicon lattice, for varying volume compaction and different compacted layer thicknesses. From this estimation it can be concluded that compaction induces stress can account for the measured resonance wavelength shift of about 5 nm.

Although all experiments in this report were performed with an electron beam, they can in principle be repeated with UV since the penetration depth at wavelengths between 200 nm and 400 nm is sufficiently low to create compaction induced strain. Ring resonators in other semiconductor materials can be compacted in a similar way, as well as other kinds of cavities, such as photonic crystal cavities.

5. Conclusions

We report on the trimming of a silicon ring resonator by electron beam irradiation. The oxide cladding is subject to volume compaction, causing tensile strain in the silicon lattice. Both effects generate an increase in refractive index, generating a red shift in resonance wavelength. The dominant effect is the tensile strain in silicon, since we have estimated a maximum contribution of 0.5 nm due to oxide refractive index changes (due to limited confinement in the cladding). In our experiment we have measured a maximum resonance wavelength red shift of 5 nm. In spite of a decrease in Q-factor for large resonance wavelength shifts and an ageing effect to be investigated we believe that this technique compensate for variations on wafer scale and on chip scale due to optical lithography imperfections. Specifically in combination with vertical grating couplers and in live readout, this technique is suited for rapid and automatic trimming of devices before packaging and on wafer scale.

Acknowledgments

This work was partly supported by the European Union through the Network of Excellence ePIXnet, by the Belgian IAP-PHOTON network and the Fund for Scientific Research (FWO).